materials

MDPI

Article

The Role of Different Alkali Metals in the $A_{15}Tl_{27}$ Type Structure and the Synthesis and X-ray Structure Analysis of a New Substitutional Variant $Cs_{14.53}Tl_{28.4}$

Vanessa F. Schwinghammer [1], Susanne M. Tiefenthaler [1] and Stefanie Gärtner [1,2,*]

[1] Institute of Inorganic Chemistry, University of Regensburg, 93040 Regensburg, Germany; Vanessa.Schwinghammer@ur.de (V.F.S.); Susanne.Tiefenthaler@ur.de (S.M.T.)
[2] Central Analytics, X-ray Crystallography Department, University of Regensburg, 93040 Regensburg, Germany
* Correspondence: Stefanie.Gaertner@ur.de; Tel.: +49-941-943-4446

Abstract: Alkali metal thallides have been known since the report of E. Zintl on NaTl in 1932. Subsequently, binary and ternary thallides of alkali metals have been characterized. At an alkali metal proportion of approximately 33% (A:Tl~1:2, A = alkali metal), three different unique type structures are reported: $K_{49}Tl_{108}$, $Rb_{17}Tl_{41}$ and $A_{15}Tl_{27}$ (A = Rb, Cs). Whereas $Rb_{17}Tl_{41}$ and $K_{49}Tl_{108}$ feature a three-dimensional sublattice of Tl atoms, the $A_{15}Tl_{27}$ structure type includes isolated Tl_{11} clusters as well as two-dimensional Tl-layers. This unique arrangement is only known so far when the heavier alkali metals Rb and Cs are included. In our contribution, we present single-crystal X-ray structure analyses of new ternary and quaternary compounds of the $A_{15}Tl_{27}$ type structure, which include different amounts of potassium. The crystal structures allow for the discussion of the favored alkali metal for each of the four Wyckoff positions and clearly demonstrate alkali metal dependent site preferences. Thereby, the compound $Cs_{2.27}K_{12.73}Tl_{27}$ unambiguously proves the possibility of a potassium-rich $A_{15}Tl_{27}$ phase, even though a small amount of cesium appears to be needed for the stabilization of the latter structure type. Furthermore, we also present two compounds that show an embedding of Tl instead of alkali metal into the two-dimensional substructure, being equivalent to the formal oxidation of the latter. $Cs_{14.53}Tl_{28.4}$ represents the binary compound with the so far largest proportion of incorporated Tl in the structure type $A_{15}Tl_{27}$.

Keywords: thallide; intermetallics; single crystal; X-ray structure analysis

Citation: Schwinghammer, V.F.; Tiefenthaler, S.M.; Gärtner, S. The Role of Different Alkali Metals in the $A_{15}Tl_{27}$ Type Structure and the Synthesis and X-ray Structure Analysis of a New Substitutional Variant $Cs_{14.53}Tl_{28.4}$. *Materials* **2021**, *14*, 7512. https://doi.org/10.3390/ma14247512

Academic Editor: Simon Steinberg

Received: 29 October 2021
Accepted: 29 November 2021
Published: 8 December 2021

1. Introduction

Alkali metal thallides represent a very interesting class of materials in terms of structural chemistry as they involve versatile thallium substructures depending on the amount of alkali metal involved, which is equitable to the valence electron concentration [1]. The electronic description of the latter compounds is not trivial, as part of them are diamagnetic and show a real band gap; therefore, the description by the Zintl-Klemm formalism is permissible in a narrow sense [2–5]. In contrast, quite a large number of these compounds show metallic and paramagnetic behavior [6,7] and the basis of this concept, the complete electron transfer from the electropositive to the electronegative element, is not true for these materials. Nevertheless, in many cases, the formed anionic partial structures can be described according to this theory [8–10]. This still makes this concept a very powerful tool in solid state chemistry at the frontier between metallic and ionic bonding. The first Zintl phase goes back to the investigations of E. Zintl, who described the crystal structure of NaTl, in which the thallium substructure follows the Zintl–Klemm formalism by forming a diamond sublattice [11]. Interestingly, thallium as a "parental" element for this concept is found left to the so-called Zintl border in the periodic table of elements [12,13]. This actually makes it a very interesting element to point out and describe structural effects of

the rather innocent electropositive counterpart on structure formation, as it can be seen as element "at the boundary of the border". Alkali metal thallides experienced a renaissance due to the investigations of *J. D. Corbett* in the 1990's [8,9]. One of the type structures he reported on in 1996 is $A_{15}Tl_{27}$, which could be realized for the heavier congeners rubidium and cesium [14]. The crystal structures of these compounds showed the involvement of two thallium substructures. On the one hand, discrete Tl_{11}^{7-} clusters are present, which are also known from binary A_8Tl_{11} (A=K, Rb, Cs) phases crystallizing in the K_8In_{11}-type structure [7,15]. In these compounds, an extra electron is present $A_8[Tr_{11}^{7-}][e^-]$ being responsible for pauli paramagnetism and metallic behavior. This extra electron can be replaced by halide in $A_8Tr_{11}X$, and for $Cs_8Ga_{11}Cl$ diamagnetic behavior is observed [16–19]. Detailed investigations on $A_8Tl_{11}X$ showed that this replacement is accompanied by a less pronounced distortion of the Tl_{11} clusters from ideal D_{3h} symmetry [17,18]. In general, Tl_{11}^{7-} clusters represent a favored geometry as they also can be perceived as double-tetrahedral star units, which represent a very common structural motif in intermetallic compounds [20]. For example, in $K_{18}Tl_{20}Au_3$ as molecular building blocks also Tl_{11}^{7-} cluster anions and additional $Tl_9Au_2^{9-}$ polyanions are present [21]. Due to the high symmetry of the hexagonal crystal structure of the latter, the point group of the Tl_{11} cluster in this case is D_{3h}. In the here investigated $A_{15}Tl_{27}$ compounds, beside the Tl_{11} clusters, an additional subunit of thallium atoms is present, two-dimensional Tl_{16}^{8-} layers, which include large pores, in which alkali metal atoms reside [14]. In the compound $Rb_{14}CsTl_{27}$, the preference of the larger alkali metal cesium residing in the pore was proven. A related compound to the $A_{15}Tl_{27}$ type structure was reported in 1997 for $K_{14}Cd_9Tl_{21}$. Here, one symmetry inequivalent thallium site of the layer was replaced by one cadmium atom. Additionally, the alkali metal position being located in the pore could be substituted by a Cd_3 triangle, which gave rise to the formation of two-dimensional $[Cd_9Tl_{10}]^{7-}$ layers [22]. Band structure and extended Hückel calculations indicated a two-dimensional metal for the latter compound. Whereas in $K_{14}Cd_9Tl_{21}$ potassium acts as counter cation, binary $K_{15}Tl_{27}$ has not yet been reported. In contrast, for binary thallides with an alkali metal content of appr. 0.3, for potassium only $K_{49}Tl_{108}$ is reported [23]. This compound includes a three-dimensional thallium network. The change from potassium to larger, more electropositive alkali metals accounts for a change in the type of structure accompanied by a significant change in the thallium sublattice. A similar dependency on the alkali metal involved has previously been reported for ATl (A=Li-Cs) [8,9,11,24–28]. In the region of A:Tl (1:2) the absence of $K_{15}Tl_{27}$ [14] on the one hand and on the other hand the observation of $K_{49}Tl_{108}$ [23,29] makes compositions, including different alkali metals, very promising candidates for the investigations of the influence of the latter on structure formation. In the search of a composition near $K_{15}Tl_{27}$, we here report on different ternary and a quaternary $A_{15}Tl_{27}$ phases, including potassium. The influence of the mixed alkali metals on the thallium substructure is discussed. Additionally, the compounds $Cs_{14.53}Tl_{28.4}$ and $Cs_{8.21}Rb_{6.76}Tl_{27.09}$ give the first evidence, that replacement of the alkali metal in the pores of the two-dimensional layer in $Cs_{15}Tl_{27}$ by thallium is possible.

2. Materials and Methods

All compounds have been prepared by using classical solid-state techniques. The alkali metals cesium and rubidium were obtained by reduction in the alkali metal chlorides with elemental calcium [30] and afterwards distilled twice for purification. Potassium was segregated for purification. Thallium drops (ABCR, purity 99.99%) were used without further purification and were stored under inert gas atmosphere. The starting materials were placed in tantalum ampoules and sealed in argon atmosphere. The sealed crucibles were afterwards placed in quartz glass tubes (QSIL GmbH, Ilmenau, Germany) and sealed under argon atmosphere. The same temperature program was used for all compounds: heating up to 973.15 K with a heating rate of 100 K/h, holding for 24 h, cooling to room temperature with a cooling rate of 3 K/h.

The received products are very sensitive towards moisture and oxygen; therefore, they were stored in a glove box (Labmaster 130 G Fa. M. Braun, Garching, Germany). In advance of the characterization by single crystal X-ray diffraction techniques, a small number of crystals was transferred into dried mineral oil. Subsequently, a suitable crystal was isolated and mounted on the Rigaku SuperNova diffractometer (Rigaku Polska Sp. Z o. o. Ul, Wroclaw, Poland) (X-ray: Mo-source, Eos detector) using MiTeGen loops, before collecting data at 123 K. The program CrysAlisPro was used for data collection and data reduction [31]. The solution of the structure and subsequent refinements were accomplished in Olex2 [32] using ShelXT [33,34]. For generating representations of the crystal structures, the software Diamond was used [35].

Powder diffraction samples were prepared in sealed capillaries (ø 0.3 mm, WJM-Glas-Müller GmbH, Berlin, Germany) and data collection was performed on a STOE Stadi P diffractometer (STOE, Darmstadt, Germany) (monochromatic Mo-$K_{\alpha 1}$ radiation λ = 0.70926 Å) equipped with a Dectris Mythen 1 K detector. The visualization and indexation was carried out by the software WinXPOW [36].

3. Results

All compounds crystallize in the $A_{15}Tl_{27}$ (A = Cs, Rb)-type structure (hexagonal, space group *P*-62*m*) [14]. These alkali metal thallides naturally possess very high absorption coefficients (MoKα, $\mu > 70$ mm^{-1}), hence small single crystals were selected for the X-ray diffraction experiments, but the data sets still suffered from severe absorption effects, which could be reduced by applying absorption correction. The high redundancy of the collected data sets additionally allowed a shape adjustment by the "shape optimization" tool in the CrysAlisPro software (diffractometer software, Rigaku).

We first observed the evidence of the mixed $A_{15}Tl_{27}$ phases ($K_{6.96}Rb_{8.04}Tl_{27}$ and $Cs_{8.21}Rb_{6.76}Tl_{27.09}$) during our studies concerning $A_8T_{11}X$ compounds, where they crystallized as a by-product together with $K_{3.98}Rb_{4.02}Tl_{11}Cl_{0.1}$ and $Cs_{5.13}Rb_{2.87}Tl_{11}Cl_{0.49}$, respectively. The smaller amount of incorporated chloride in these compounds, which simultaneously means a higher degree of reduction, facilitated the formation of the less reduced $A_{15}Tl_{27}$ phases, which include less alkali metal per Tl. As the results of these crystal structure determinations allowed deeper insights in the alkali metal dependent site preferences, we subsequently started to prepare and characterize mixed alkali metal approaches following the composition $A_{15}Tl_{27}$ (A = K, Rb, Cs). Table 1 shows the data of the structure determinations of all approaches, including potassium and at least one other alkali metal.

Table 1. Crystal data and structure refinement details of the approaches to obtain binary $K_{15}Tl_{27}$.

Empirical Formula	**$K_{6.96}Rb_{8.04}Tl_{27}$**	**$Cs_{5.92}K_{9.08}Tl_{27}$**	**$Cs_{2.27}K_{12.73}Tl_{27}$**	**$Cs_{3.57}K_{4.55}Rb_{6.92}Tl_{27}$**
CSD number *	2088508	2093385	2093386	2093391
Formula weight	6477.30	6659.84	6318.00	6761.84
Temperature (K)	123	123	123	123
Crystal system	hexagonal	hexagonal	hexagonal	hexagonal
Space group	*P*-62*m*	*P*-62*m*	*P*-62*m*	*P*-62*m*
a (Å)	10.1835(2)	10.2542(4)	10.20330(10)	10.30543(11)
c (Å)	17.1041(4)	17.0278(12)	16.7702(2)	17.2475(2)
α (°)	90	90	90	90
γ (°)	120	120	120	120
Volume (Å^3)	1536.12(7)	1550.57(17)	1511.99(3)	1586.31(4)
c/*a*	1.68	1.66	1.64	1.67
Z	1	1	1	1
ρ_{calc} (g/cm$^{3)}$	7.002	7.132	6.938	7.078
μ (mm^{-1})	77.292	73.869	73.847	75.853
F(000)	2617.0	2685.0	2554.0	2726.0
Crystal size (mm^3)	0.12 × 0.09 × 0.08	0.183 × 0.113 × 0.044	0.093 × 0.058 × 0.04	0.105 × 0.051 × 0.039

Table 1. *Cont.*

Empirical Formula	$K_{6.96}Rb_{8.04}Tl_{27}$	$Cs_{5.92}K_{9.08}Tl_{27}$	$Cs_{2.27}K_{12.73}Tl_{27}$	$Cs_{3.57}K_{4.55}Rb_{6.92}Tl_{27}$
Radiation	MoKα (λ = 0.71073)	MoKα (λ = 0.71073)	MoKα (λ = 0.71073)	MoKα (λ = 0.71073)
2Θ range for data collection (°)	6.636 to 59.01	6.63 to 59.508	6.698 to 70.162	6.57 to 72.68
Index ranges	$-10 \leq h \leq 12$ $-13 \leq k \leq 5$ $-11 \leq l \leq 23$	$-13 \leq h \leq 14$ $-11 \leq k \leq 12$ $-23 \leq l \leq 23$	$-16 \leq h \leq 16$ $-16 \leq k \leq 16$ $-27 \leq l \leq 26$	$-16 \leq h \leq 17$ $-17 \leq k \leq 17$ $-28 \leq l \leq 28$
Reflections collected	3380	7018	97696	103808
Independent reflections	1431	1526	2479	2828
Data/restraints/parameters	1431/0/48	1526/0/47	2479/0/47	2828/3/52
Goodness-of-fit on F^2	1.079	1.111	1.359	1.235
R_{int}	R_{int} = 0.0352	R_{int} = 0.0660	R_{int} = 0.0481	R_{int} = 0.0611
Final R indexes [I >= 2σ (I)]	R1 = 0.0419 wR2 = 0.1003	R1 = 0.0345 wR2 = 0.0631	R1 = 0.0173 wR2 = 0.0504	R1 = 0.0208 wR2 = 0.0592
Final R indexes [all data]	R1 = 0.0442 wR2 = 0.1031	R1 = 0.0404 wR2 = 0.0655	R1 = 0.0185 wR2 = 0.0506	R1 = 0.0221 wR2 = 0.0596
Largest diff. peak/hole (e $Å^{-3}$)	2.04/−1.94	2.59/−2.62	3.37/−2.07	2.78/−2.06
Flack parameter	0.03(7)	−0.006(16)	0.005(4)	0.003(5)

* Further details of the crystal structure investigation(s) may be obtained free of charge from the Cambridge Crystallographic Data Centre CCDC (Access Structures) on quoting the deposition number (given in the table) CSD-xxxxxx or the the deposition number CCDC-xxxxxxx.

For the ternary approaches including potassium, we additionally obtained the less reduced $A_{49}Tl_{108}$ phases as side products [15,23]. This is reasonable, as the amount of alkali metal is very similar in both compounds (0.357 for $A_{15}Tl_{27}$ and 0.312 for $K_{49}Tl_{108}$). Additionally, we observed formations of multicrystals between the $A_{15}Tl_{27}$ and $A_{49}Tl_{108}$ phases. This might be due to the fact that the longest side of the unit cell of the $A_{15}Tl_{27}$ and the cell vector of the $A_{49}Tl_{108}$ (cubic, *Pm*-3, a~17Å) are close in length.

$Cs_{8.21}Rb_{6.76}Tl_{27.09}$ exhibits residual electron density near the alkali metal position A4 (d(A4-q) > 2.7 Å), for which the assignment of Tl is reasonable in terms of the observed Tl-Tl distances (see Section 4.3 Discussion). However, the obtained s.o.f. of less than 10% thallium made this interpretation suspicious; therefore, binary samples involving cesium and a higher amount of thallium were prepared which all led to the composition $Cs_{14.53}Tl_{28.4}$. *Corbett*'s $Cs_{15}Tl_{27}$ was prepared in addition and the absence of additional thallium in this phase was confirmed. Table 2 gives the data of the structure solution and refinement of $Cs_{8.21}Rb_{6.76}Tl_{27.09}$, $Cs_{14.53}Tl_{28.4}$ and $Cs_{15}Tl_{27}$.

Table 2. Crystal data and structure refinement details of the approaches with incorporated Tl.

Empirical Formula	$Cs_{8.21}Rb_{6.76}Tl_{27.09}$	$Cs_{14.53}Tl_{28.4}$	$Cs_{15}Tl_{27}$
CSD number *	2088490	2088509	2088513
Formula weight	7205.35	7735.60	7511.64
Temperature (K)	122.99(10)	123.00(16)	123.00(18)
Crystal system	hexagonal	hexagonal	hexagonal
Space group	*P*-62*m*	*P*-62*m*	*P*-62*m*
a (Å)	10.3383(4)	10.5007(3)	10.4240(7)
c (Å)	17.6308(9)	17.9963(6)	18.0525(16)
α (°)	90	90	90
γ (°)	120	120	120
Volume ($Å^3$)	1631.93(15)	1718.50(11)	1698.8(3)
c/a	1.71	1.71	1.73
Z	1	1	2
ρ_{calc} (g/cm^3)	7.332	7.474	14.685
μ (mm^{-1})	76.096	73.862	143.327
F(000)	2896.0	3100.0	6024.0

Table 2. *Cont.*

Empirical Formula	$Cs_{8.21}Rb_{6.76}Tl_{27.09}$	$Cs_{14.53}Tl_{28.4}$	$Cs_{15}Tl_{27}$
Crystal size (mm^3)	0.06 × 0.05 × 0.04	0.051 × 0.045 × 0.036	0.05 × 0.032 × 0.016
Radiation	MoKα (λ = 0.71073)	MoKα (λ = 0.71073)	MoKα (λ = 0.71073)
2Θ range for data collection (°)	6.486 to 59.35	7.762 to 66.274	7.82 to 56.438
Index ranges	$-13 \leq h \leq 13$, $-13 \leq k \leq 13$, $-24 \leq l \leq 14$	$-16 \leq h \leq 15$, $-16 \leq k \leq 16$, $-27 \leq l \leq 26$	$-11 \leq h \leq 12$, $-13 \leq k \leq 13$, $-21 \leq l \leq 24$
Reflections collected	4416	14514	8330
Independent reflections	1536	2408	1570
Data/restraints/parameters	1536/0/50	2408/6/56	1570/0/45
Goodness-of-fit on F^2	1.178	1.062	1.069
R_{int}	R_{int} = 0.0377	R_{int} = 0.0473	R_{int} = 0.0881
Final R indexes [I >= 2σ (I)]	R1 = 0.0333 wR2 = 0.0656	R1 = 0.0281 wR2 = 0.0591	R1 = 0.0376 wR2 = 0.0634
Final R indexes [all data]	R1 = 0.0384 wR2 = 0.0675	R1 = 0.0325 wR2 = 0.0606	R1 = 0.0495 wR2 = 0.0671
Largest diff. peak/hole (e $Å^{-3}$)	3.12/−2.33	1.48/−1.51	2.42/−2.30
Flack parameter	0.002(16)	−0.004(9)	−0.017(19)

* Further details of the crystal structure investigation(s) may be obtained free of charge from the Cambridge Crystallographic Data Centre CCDC (Access Structures) on quoting the deposition number (given in the table) CSD-xxxxxx or the the deposition number CCDC-xxxxxxx.

The refinement of $Cs_{14.53}Tl_{28.4}$ undoubtedly proves the presence of thallium beside a less occupied alkali metal position (s.o.f. 0.527(5)) which complements unity by an additional Tl site (s.o.f. 0.473(5)). Any attempt to incorporate more Tl, including a fully occupied thallium site, which would be equivalent to $Cs_{14}Tl_{30}$, always led to the composition of $Cs_{14.53}Tl_{28.4}$.

Powder diffraction patterns of $Cs_{2.27}K_{12.73}Tl_{27}$ and $Cs_{14.5}Tl_{28.4}$ were recorded (indexing and diffraction patterns see Figures S1–S3, Supplementary Material). In general, the approaches involving potassium additionally produced $A_{49}Tl_{108}$ beside $A_{15}Tl_{27}$, which could be observed in the powder diffraction patterns.

$Cs_{15}Tl_{27}$ and $Cs_{14.53}Tl_{28.4}$ naturally show very similar diffraction patterns. The indexed unit cell parameters according to the powder diffraction patterns refined to the values a = 10.8580(19) Å and c = 18.108(3) Å ($Cs_{14.5}Tl_{28.4}$) and a = 10.501(5) Å and c = 18.157(5) Å ($Cs_{15}Tl_{27}$). This confirms the trend of the unit cell parameters obtained for the single crystals. The deviations between the unit cell parameters of $Cs_{15}Tl_{27}$ and $Cs_{14.5}Tl_{28.4}$, respectively, each derived from single crystal and powder diffraction data, are due to the different applied temperatures (single crystal: 123 K; powder diffraction: room temperature (298 K)).

4. Discussion

4.1. Occupation Trends of the Alkali Metal Positions

During our search for binary $K_{15}Tl_{27}$ and the role of the different alkali metal sites in $A_{15}Tl_{27}$ in general, different ternary and quaternary approaches were applied. Those new compounds gave insight into the site preferences of the different alkali metals. In $A_{15}Tl_{27}$, four different alkali metal sites are present (see Figure 1). Corbett et al. showed for $Rb_{14}CsTl_{27}$, that cesium preferably resides at position A4, as the rather large pore within the two-dimensional layer allows more space for the larger alkali metal [14]. By having a closer look at the surroundings of the remaining alkali metals, additional site preferences would be conceivable [1]. In further detail, the alkali metal positions A1 and A3 are distinguished from A2 and A4 by their number and distances of surrounding atoms, which is also reflected in their crystallographic site symmetry (see Figure 1). Alkali metals on the Wyckoff-position 6*i* separate the Tl-layer from the isolated Tl_{11} clusters. Here, less contacts within a smaller range of distances are observed, whereas alkali metal atoms on position 1*b* (within the pores of the Tl-layer) and 2*c* (between the isolated clusters) show

larger distances to a higher number of neighboring atoms [1,14]. As the positions A2 and A4 show contacts to a larger number of neighboring atoms and additionally more space around them is available, they are likely to be preferable positions for the heavier alkali metals. This assumption can be reinforced by the new ternary and quaternary compounds (Table 3). The distances from alkali metal to thallium atoms naturally increases with increasing size of the alkali metal. This trend is also reflected in the unit cell parameters. Larger alkali metals on position A2 and A4 result in an increased value for the a-axis, whereas smaller alkali metals on A1 and A3 result in decreasing values for c. This compression along c upon an increasing content of potassium is also reflected in the decreasing *c/a* value (Tables 1 and 2).

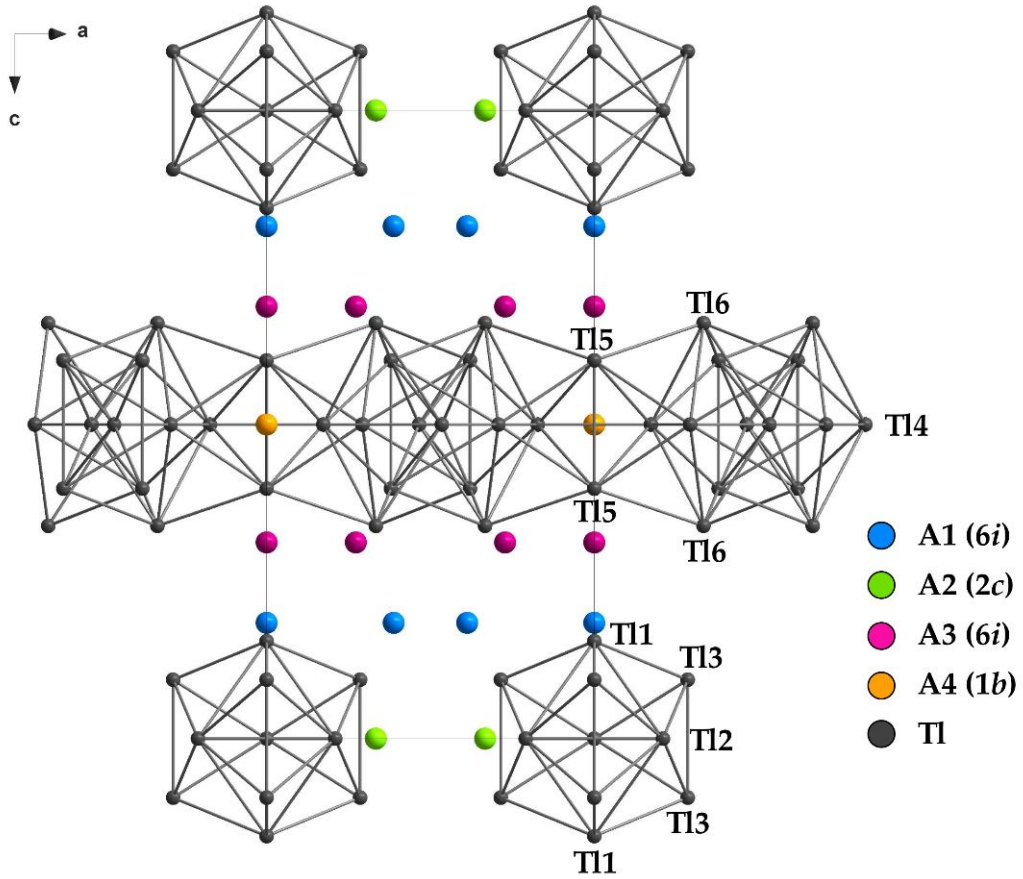

Figure 1. Unit cell of the $A_{15}Tl_{27}$ type structure with the 4 symmetry-independent alkali metal positions.

Table 3. Site occupancy factors (s.o.f.) of the symmetry-independent alkali metal positions of the mixed alkali metal thallides of the $A_{15}Tl_{27}$ type structure.

Compound	A1 (6*i*)	A2 (2*c*)	A3 (6*i*)	A4 (1*b*)	d(Tl4-A4) (Å) d(Tl5-A4) (Å)
$Cs_{8.21}Rb_{6.76}Tl_{27.09}$	Cs 0.57(2) Rb 0.43(2)	Cs	Cs 0.31(2) Rb 0.69(2)	Cs 0.970(7) Tl 0.030(7)	4.2212(11) 4.2995(12)
$K_{6.96}Rb_{8.04}Tl_{27}$	K 0.45(3) Rb 0.55(3)	Rb	K 0.68(3) Rb 0.32(3)	K 0.18(6) Rb 0.82(6)	4.1369(13) 4.2369(15)
$Cs_{5.85}K_{9.15}Tl_{27}$	Cs 0.368(10) K 0.632(10)	Cs	Cs 0.119(9) K 0.881(9)	Cs	4.1786(9) 4.2623(11)
$Cs_{2.27}K_{12.73}Tl_{27}$	K	Cs 0.665(13) K 0.335(13)	K	Cs	4.1475(5) 4.2584(5)
$Cs_{3.57}K_{4.55}Rb_{6.92}Tl_{27}$	Cs 0.18(3) Rb 0.56(5) K 0.26(3)	Cs 0.75(3) Rb 0.25(4)	Rb 0.508(16) K 0.49(3)	Cs	4.1996(5) 4.2885(6)

The values for the quaternary compound in Tables 1 and 3 represent our best possible model for the structure solution involving three different alkali metals yielding the sum formula $Cs_{3.57}K_{4.55}Rb_{6.92}Tl_{27}$. Of course, a definitive statement about the alkali metal proportions, when three alkali metals are involved, is not possible; therefore, this compound is listed, but will not be discussed in detail.

In general, the size of the pore, which is reflected in the Tl4-A4 and Tl5-A4 distances (Table 3), is not only affected by the size of the (mixed) alkali metals on position A4, but also by the differently occupied remaining alkali metal sites.

The layer and the cluster separating positions A1 and A3 show fewer contacts within smaller distances, which is equitable to a smaller void; therefore, a preferred occupation by lighter alkali metals should be expected. This can be confirmed by the observed compounds. Again, the occupation tendencies differ for both sites. The alkali metal position next to the two-dimensional Tl_{16}^{8-} layer (A3) consistently shows a higher amount of lighter alkali metals than the one next to the Tl_{11} clusters (A1). This is in accordance with the surroundings of A1 and A3, as the distances between the thallium atoms and A3 are smaller (<4.14 Å) than the Tl-A1 distances (d(Tl-A1) < 4.29 Å). In other words, the smallest void is observed around A3, where preferably smaller alkali metal resides.

4.2. Influence of Mixed Alkali Metal Sites on the Thallium Substructures

In $A_{15}Tl_{27}$, isolated Tl_{11} clusters are present; additionally, the two-dimensional layer which can be regarded as connected Tl_{11} clusters via common Tl5-Tl5 edges (Figure 2) is also present.

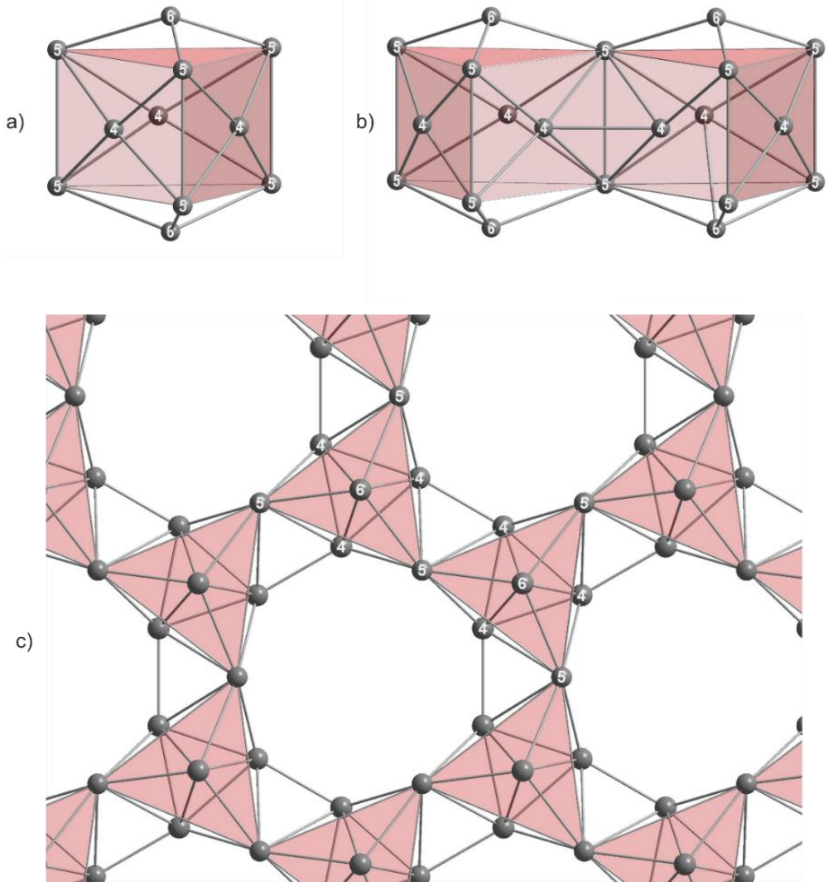

Figure 2. The two-dimensional layer in $A_{15}Tl_{27}$ type structures consists of Tl_{11} clusters (**a**) which are interconnected by a common Tl5-Tl5 edge and a Tl4-Tl4 inter-cluster distance is formed (**b**). Altogether, six Tl_{11} cluster entities define the pore (**c**). In $A_{15}Tl_{27}$, this pore is filled by alkali metal. $Cs_{8.21}Rb_{6.76}Tl_{27.09}$ and $Cs_{14.53}Tl_{28.4}$ prove the possibility of substituting this alkali metal position by thallium. Selected distances for both compounds are given in Table 5.

By comparing those two different Tl_{11} entities, the Tl3-Tl3 distances (isolated Tl_{11}^{7-}) and Tl5-Tl5 distances (Tl_{16}^{8-} layer) refer to the stretching or compression of the clusters in horizontal and vertical directions (Figure 3a,b).

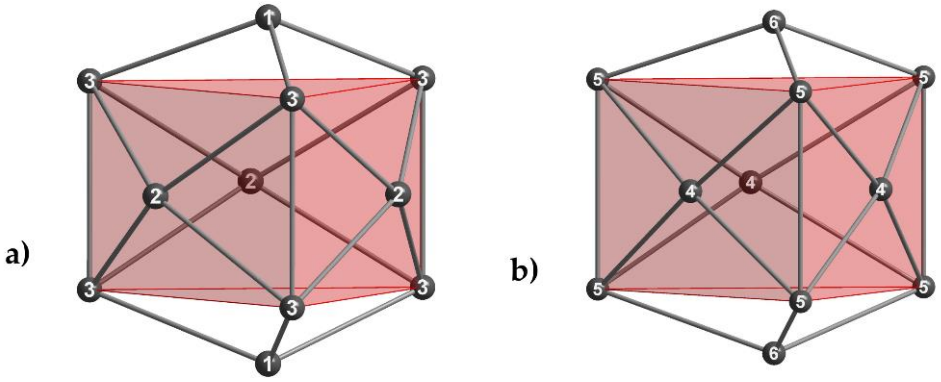

Figure 3. (**a**) isolated Tl_{11} cluster and (**b**) Tl_{11} cluster of the two-dimensional layer.

For the isolated Tl_{11} clusters (Figure 3a, Table 4), the distance from the trigonal prism (Tl3) to the quadrangular face capping Tl2 atoms increases, whereas the distance between the Tl3 atoms diminishes when the potassium proportion is enlarged. This is according to the observed *c/a* value for the unit cell parameters. Generally, Tl3-Tl3 distances in the isolated clusters are shorter compared with the Tl5-Tl5 distances of the fused clusters within the layer, which already was observed by *Corbett* in his three compounds ($Rb_{15}Tl_{27}$, $Cs_{15}Tl_{27}$ and $Rb_{14}CsTl_{27}$) [14]. This trend can be confirmed for our ternary and quaternary thallides.

Table 4. Dimensions of the isolated Tl_{11}-clusters in $A_{15}Tl_{27}$ structure type.

Compound	d(Tl2-Tl2) (Å)	d(Tl3-Tl3) (Å)	d(Tl2-Tl3) (Å)
$Cs_{8.21}Rb_{6.76}Tl_{27.09}$	3.749(3)	3.202(2)	3.0710(10)
$K_{6.96}Rb_{8.04}Tl_{27}$	3.753(3)	3.198(2)	3.0855(11)
$Cs_{5.85}K_{9.15}Tl_{27}$	3.721(2)	3.197(2)	3.0731(9)
$Cs_{2.27}K_{12.73}Tl_{27}$	3.7333(12)	3.1908(10)	3.0926(4)
$Cs_{14.53}Tl_{28.4}$	3.7697(16)	3.2146(13)	3.0833(6)
$Cs_{15}Tl_{27}$	3.774(3)	3.212(3)	3.0816(12)

Ideal Tl_{11}^{7-} clusters exhibit D_{3h} symmetry. In contrast, the Tl_{11} cluster fragment of the two-dimensional layer shows C_{3h} symmetry due to missing vertical mirror planes for this point group. As a result, two different values for Tl4-Tl5 distances are observed. For the evaluation of the distortion of the layer, the deviation from C_{3h} to the higher D_{3h} symmetry can be taken into account. For this purpose, we already introduced a cdd/cd_{av} ratio (*cdd*: capping distance difference; cd_{av}: average capping distance; Equation (1)) for isolated Tl_{11}^{7-} clusters [18], which allows a quick estimation of the degree of distortion. This approach was employed again in order to gain deeper insight in the degree of distortion of the layer-forming Tl_{11} entities.

$$\frac{cdd}{cd_{av}} = \frac{|cd_2 - cd_1|}{\left(\frac{cd_2+cd_1}{2}\right)} \quad with\ cd_1 \leq\ cd_2 \tag{1}$$

It becomes apparent, that as soon as potassium is present, the degree of distortion gives larger values compared with compounds without potassium. The K-Rb approach shows the greatest degree of distortion with almost 7%. This indicates that additional distortion can be expected when rubidium is used instead of cesium, which we focused on in our current investigations. Considering the Cs-K approaches, the degree of distortion increases with increasing potassium content (Table 5). Therefore, the substitution of cesium by lighter alkali metals has a clear influence on the two-dimensional Tl layer structure.

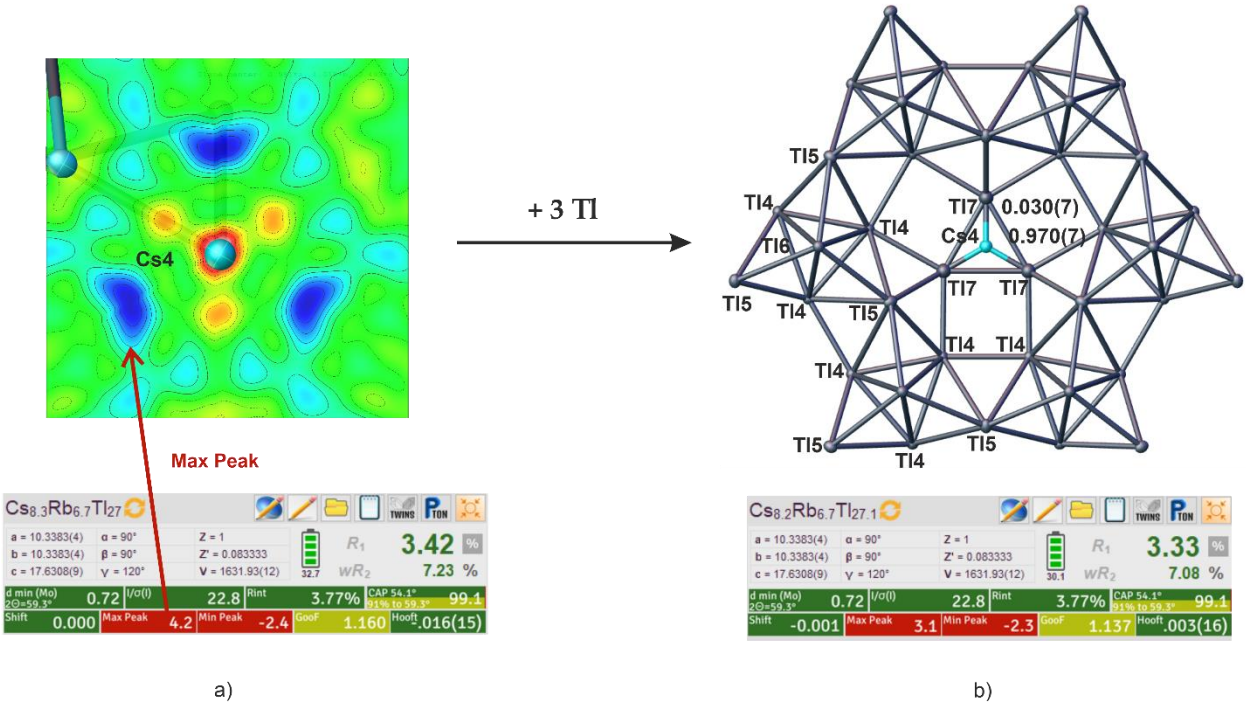

Figure 4. (**a**) Electron density map generated by Olex2 (see Section 2) of the area around Cs4 shows surrounding residual density (blue), which created the idea of additional thallium being partially present instead of Cs4. (**b**) The partial replacement of Cs4 (Wyckoff 1b) by Tl7 (Wyckoff 3g) results in two subunits being present in $Cs_{8.21}Rb_{6.76}Tl_{27.1}$: cesium, including Tl_{16}^{8-} layers and cesium-free Tl_{19}^{7-} layers. Refinement indicators (Olex2) show improved model for $Cs_{8.21}Rb_{6.76}Tl_{27.1}$.

Table 5. Dimensions of the Tl_{11} clusters in the two-dimensional layers of the $A_{15}Tl_{27}$ type structure. The atom numbers are according to the numbering scheme in Figure 4. A and B indicate the split positions of Tl5.

Compound	d(Tl6-Tl5) (Å)	d(Tl5-Tl5) (Å)	d(Tl4-Tl4) (Å)	d(Tl4-Tl5) (Å)	d(Tl4-Tl5#) (Å)	d(Tl4-Tl6) (Å)	$\frac{cdd}{cd_{av}}$ (%)	*c*/*a*
$Cs_{8.21}Rb_{6.76}Tl_{27.09}$	3.3735(7)	3.463(2)	3.2924(19) 3.088(2)	3.2122(11)	3.3917(14)	3.3078(13)	5.44	1.71
$K_{6.96}Rb_{8.04}Tl_{27}$	3.3423(8)	3.533(2)	3.270(2) 3.040(3)	3.1796(13)	3.4068(17)	3.3450(15)	6.90	1.68
$Cs_{5.85}K_{9.15}Tl_{27}$	3.3622(7)	3.475(2)	3.2721(16) 3.0713(19)	3.1860(10)	3.3923(12)	3.3329(13)	6.27	1.66
$Cs_{2.27}K_{12.73}Tl_{27}$	3.3493(3)	3.5211(9)	3.2665(8) 3.0606(9)	3.1798(5)	3.3981(6)	3.3611(5)	6.64	1.64
$Cs_{14.53}Tl_{28.4}$	3.3093(15) (A) 3.4628(19) (B)	3.627(10) (A) 3.457(11) (B)	3.2860(14) 3.1423(15)	3.242(4) (A) 3.259(3) (B)	3.385(3) (A) 3.465(4) (B)	3.3170(8)	4.32 6.13	1.71
$Cs_{15}Tl_{27}$	3.3940(8)	3.457(3)	3.322(2) 3.102(3)	3.2361(14)	3.4039(17)	3.3026(16)	5.05	1.73

4.3. Effects of Incorporation of Tl in the Two-Dimensional Layers

The large pores in the two-dimensional layer were shown to be preferably occupied by larger alkali metals. In $K_{14}Cd_9Tl_{21}$ [22], it was reported, that instead of alkali metal also cadmium can be present, yielding an alkali metal-free $[Cd_9Tl_{10}]^{7-}$ layer. Unusually large residual electron density beside cesium in cadmium-free $Cs_{8.22}Rb_{6.75}Tl_{27.09}$ created the idea that it might be possible to introduce thallium in this place. In this compound, the electron density was refined to a value of 3% for thallium (see Figure 4), which of course does not prove this theory.

Subsequently, larger amounts of thallium were employed during the solid-state synthesis to prove the idea of thallium being embedded into the pores of the Tl_{16}^{8-} layers of $Cs_{15}Tl_{27}$ (see Section 3. Results). The obtained single crystals undoubtedly confirmed

the presence of additional thallium in the pores to an extent of 0.473(5). The s.o.f.'s of Cs4 accordingly reduced to 0.527(5)). Additionally, split positions for Tl5 could be refined, which are induced by the thallium incorporation in the pore (Figures 5 and 6). This leads to two settings being present in $Cs_{14.53}Tl_{28.4}$: On the one hand a pore description is obtained, equivalent to $Cs_{15}Tl_{27}$, with two-dimensional $[Tl_{16}]^{8-}$ layers with cesium (Cs4, 1*b*) residing in the pore (Figure 5a). On the other hand, pores are present, where instead of cesium on the Wyckoff position 1*b*, three thallium atoms (Tl7, 3*g*) are present in the $[Tl_{19}]^{7-}$ layer (Figure 5b). The assignment of the charge of the layer is due to the known charge of the Tl_{11}^{7-} clusters [14] and by assuming a complete electron transfer from the alkali metal to thallium, which is according to the approach of *Tillard* et al. and *Corbett* et al. In comparison with the cadmium compound, where Cd2 atoms form a triangle in the pores, the distances between the Tl7 atoms in our triangle are longer (d(Cd2-Cd2) = 2.816(7) Å [22], d(Tl7-Tl7) = 3.126(4) Å). The two symmetrically inequivalent Tl4-Tl4 distances in $Cs_{14.53}Tl_{28.4}$ (3.2860(14) Å and 3.1423(15) Å) become more similar compared with Tl4-Tl4 in $Cs_{15}Tl_{27}$ (3.322(2) Å and 3.102(3) Å). In the related compound $K_{14}Cd_9Tl_{21}$, a similar trend is noticed [22].

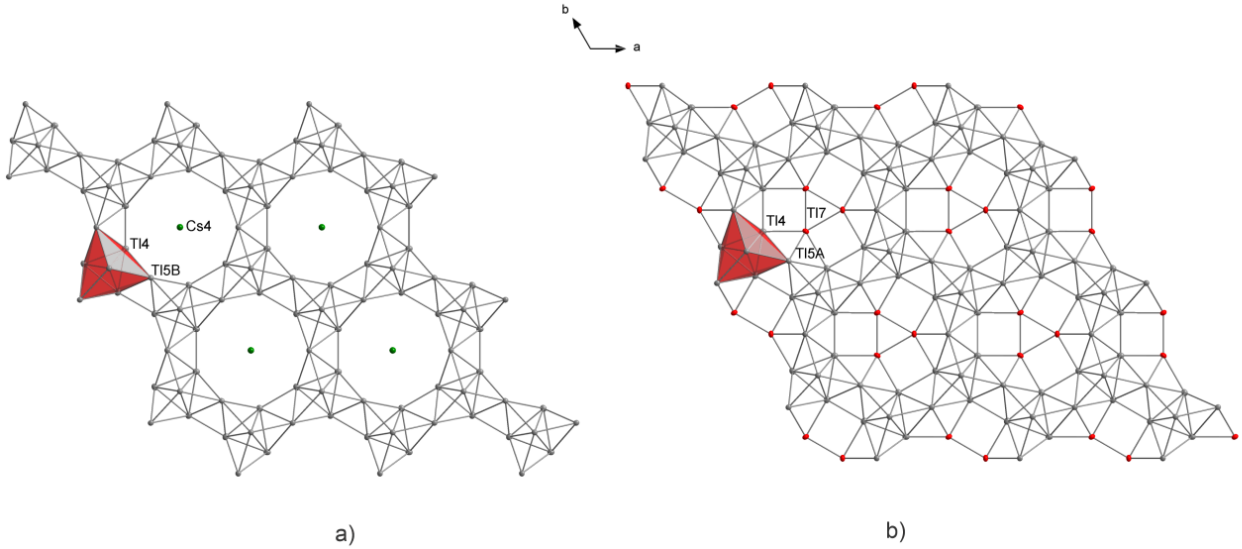

Figure 5. Different hosts in the pores of the two-dimensional layer of $A_{15}Tl_{27}$-type structures: (**a**) $Cs_{15}Tl_{27}$; (**b**) $Cs_{14.53}Tl_{28.4}$.

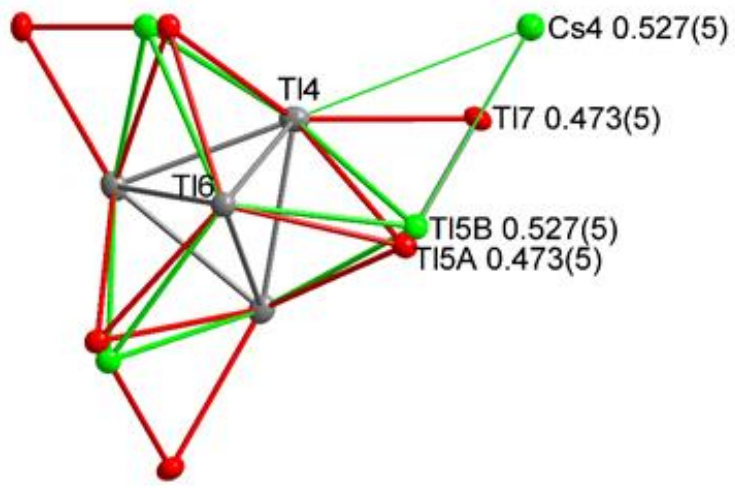

Figure 6. When Cs4 is replaced by Tl7, the unusually short Tl7-Tl5 distance would be observed. Prolate displacement of Tl5 indicated split positions, which were refined according to the s.o.f. of Tl7 and Cs4, respectively. This model yields a reasonable Tl5A-Tl7 distance and improved residual density description.

The change in the overall thallium substructure of the layer upon thallium substitution can be directly demonstrated by the position of Tl5. This position showed prolate anisotropic displacement, which could be reduced by introducing split positions. The free refinement of the split Tl positions gives s.o.f. values of 0.527(16) and 0.473(16). As these values are according to the s.o.f.s of Cs4 (0.527(5)) and Tl7 (0.473(5)), respectively, the free refinement of the split position was performed using the same s.o.f. parameter. The reason for this movement of Tl5 upon Tl substitution can be found in the newly formed Tl7-Tl5 distance: if Tl5 was not split, this would mean a short Tl5-Tl7 distance (<2.900(2) Å), which seems to be unfavorable. The splitting of this position demonstrates how the layer structure is able to respond to a change of the host in the pores. As in the above-discussed $A_{15}Tl_{27}$ compounds, a degree of distortion within the layer can be calculated. In the present case of $Cs_{14.53}Tl_{28.4}$, two different degrees of distortion are observed, as the Tl5 position is split (see Figures 5 and 6). The partial structure with the additionally embedded thallium shows a significantly smaller degree of distortion compared with all other compounds (4.3%). The second partial structure with A4 occupied by Cs gives a degree of distortion similar to that of the Cs-K phases (see Table 5).

Altogether, the formal oxidation of the former Tl_{16}^{8-} layer by forming layers of Tl_{19}^{7-} upon thallium substitution yields a less distorted thallium substructure. We observed similar effects previously for $A_8Tl_{11}X$, where less distorted Tl_{11}^{7-} was observed when halide was incorporated [18], which is equivalent to a formal oxidation of thallium in A_8Tl_{11}. A speculative compound $A_{14}Tl_{30}$ would mean that solely cesium-free layers are present. Further attempts to increase the thallium content by using the mixed alkali metal approach are currently in progress.

5. Conclusions

In summary, it can be stated that substitution of the larger alkali metals in the $A_{15}Tl_{27}$ type structure by potassium is possible to a certain extent. The presence of large alkali metals in the pores of the two-dimensional Tl_{16}^{8-} layer is essential for the stabilization of the $A_{15}Tl_{27}$ type structure. If the amount of potassium is enlarged, instead of binary $K_{15}Tl_{27}$, only $K_{49}Tl_{108}$ is observed, which is the more stable phase at appr. 1:2 (A:Tl) composition involving this lighter homologue of the alkali metals. Therefore, $Cs_{2.27}K_{12.73}Tl_{27}$ is currently the first and at the same time the potassium-richest compound found in the $A_{15}Tl_{27}$ type structure. The change in alkali metals is also reflected in the distortion of the Tl_{16}^{8-} layer structure. When cesium is involved, less distorted layer structures are observed.

Furthermore, it could be shown in $Cs_{14.53}Tl_{28.4}$, that cesium in the pore of $Cs_{15}Tl_{27}$ can be partially substituted by three thallium atoms yielding formally oxidized, less distorted two-dimensional Tl_{19}^{7-} layers.

Supplementary Materials: The following are available online at https://www.mdpi.com/article/10.3390/ma14247512/s1, Figure S1: Measured powder diffraction patterns of Cs15Tl27 (pink) and Cs14.53Tl28.4 (blue); Figure S2: Measured powder diffraction pattern of Cs 2.27 K 12.73 Tl 27 (blue) with calculated reflections of K 49 Tl 108 (pink) and of Cs 2.27 K 12.73 Tl 27from single crystal data; Figure S3: Measured powder diffraction patter of Cs 2.27 K 12.73 Tl 27 (blue, up) with calculated reflections of K 49 Tl 108 (purple, up)and calculated pattern of Cs 2.27 K 12.73 Tl 27 from single crystal (blue, down)(*) unindexed lines, impurities

Author Contributions: Conceptualization, S.G.; methodology, S.G.; software, V.F.S., S.M.T. and S.G.; formal analysis, V.F.S., S.M.T. and S.G.; investigation, V.F.S. and S.M.T.; data curation, V.F.S., S.M.T. and S.G.; writing—original draft preparation, V.F.S.; writing—review and editing, S.G. and S.M.T.; visualization, V.F.S. and S.G.; supervision, S.G.; project administration, S.G. All authors have read and agreed to the published version of the manuscript.

Funding: This research was funded by a research grant of the German Science Foundation (DFG) (GA 2504/1-1).

Institutional Review Board Statement: Not applicable.

Informed Consent Statement: Not applicable.

Data Availability Statement: Further details on the crystal structure investigation(s) may be obtained free of charge from The Cambridge Crystallographic data center CCDC (Access Structures) on quoting the deposition number given in the crystallographic tables (CSD-xxxxxx or the deposition number CCDC-xxxxxxx).

Acknowledgments: We want to thank N. Korber for providing materials and lab equipment as well as for valuable discussions and Florian Wegner for recording the powder diffraction patterns. Additionally, we want to thank C. Röhr for very helpful discussions.

Conflicts of Interest: The authors declare no conflict of interest.

References

1. Gärtner, S. Spotlight on Alkali Metals: The Structural Chemistry of Alkali Metal Thallides. *Crystals* **2020**, *10*, 1013. [CrossRef]
2. Nesper, R. The Zintl-Klemm Concept-A Historical Survey. *Z. Anorg. Allg. Chem.* **2014**, *640*, 2639–2648. [CrossRef]
3. Kauzlarich, S.M. (Ed.) *Chemistry, Structure and Bonding of Zintl Phases and Ions*; VCH Publishers, Inc.: New York, NY, USA; Weinheim, Germany, 1996.
4. Fässler, T.F. (Ed.) *Zintl Phases-Principles and Recent Developments*; Springer: Berlin/Heidelberg, Germany, 2011; Volume 139.
5. Wang, F.; Wedig, U.; Prasad, D.; Jansen, M. Deciphering the Chemical Bonding in Anionic Thallium Clusters. *J. Am. Chem. Soc.* **2012**, *134*, 19884–19894. [CrossRef] [PubMed]
6. Kaskel, S.; Corbett, J.D. Synthesis and structure of $K_{10}Tl_7$: The first binary trielide containing naked pentagonal bipyramidal Tl_7 clusters. *Inorg. Chem.* **2000**, *39*, 778–782. [CrossRef]
7. Dong, Z.-C.; Corbett, J.D. A_8Tl_{11} (A = K, Rb, or Cs) Phases with Hypoelectronic Tl_{11}^{7-} Cluster Anions: Syntheses, Structure, Bonding and Properties. *J. Clust. Sci.* **1995**, *6*, 187–201. [CrossRef]
8. Dong, Z.C.; Corbett, J.D. CsTl: A new example of tetragonally compressed Tl_6^{6-} octahedra. Electronic effects and packing requirements in the diverse structures of ATl (A = Li, Na, K, Cs). *Inorg. Chem.* **1996**, *35*, 2301–2306. [CrossRef]
9. Dong, Z.C.; Corbett, J.D. Synthesis, Structure, and Bonding of the Novel Cluster Compound KTl with Isolated Tl_6^{6-} Ions. *J. Am. Chem. Soc.* **1993**, *115*, 11299–11303. [CrossRef]
10. Smid, S.; Steinberg, S. Probing the Validity of the Zintl-Klemm Concept for Alkaline-Metal Copper Tellurides by Means of Quantum-Chemical Techniques. *Materials* **2020**, *13*, 2178. [CrossRef] [PubMed]
11. Zintl, E.; Dullenkopf, W. Über den Gitterbau von NaTl und seine Beziehung zu den Strukturen des Typus des b-Messings. *Z. Phys. Chem.* **1932**, *B16*, 195–205. [CrossRef]
12. Zintl, E.; Goubeau, J.; Dullenkopf, W. Salzartige Verbindungen und intermetallische Phasen des Natriums in flüssigem Ammoniak. *Z. Phys. Chem.* **1931**, *154*, 1–46. [CrossRef]
13. Gärtner, S.; Korber, N.; Reedijk, J.; Poeppelmeier, K. Zintl Anions. In *Comprehensive Inorganic Chemistry II*; Elsevier: Amsterdam, The Netherlands, 2013; Volume 1, pp. 251–267.
14. Dong, Z.C.; Corbett, J.D. $A_{15}Tl_{27}$ (A = Rb,Cs): A structural type containing both isolated clusters and condensed layers based on the Tl_{11} fragment. Syntheses, structure, properties, and band structure. *Inorg. Chem.* **1996**, *35*, 1444–1450. [CrossRef]
15. Blase, W.; Cordier, G.; Muller, V.; Haussermann, U.; Nesper, R.; Somer, M. Preparation and Crystal-Structures of Rb_8In_{11}, K_8Tl_{11}, and Rb_8Tl_{11} Band-Strucutre Calculations on K_8In_{11}. *Z. Naturforsch. B* **1993**, *48*, 754–760. [CrossRef]
16. Henning, R.W.; Corbett, J.D. Cs_8Ga_{11}, a new isolated cluster in a binary gallium compound. A family of valence analogues $A_8Tr_{11}X$: A = Cs, Rb; Tr = Ga, In, Tl; X = Cl, Br, I. *Inorg. Chem.* **1997**, *36*, 6045–6049. [CrossRef]
17. Gärtner, S.; Tiefenthaler, S. Single Crystal X-ray Structure Analyses of Thallides: Halide Incorporation and Mixed Alkali Sites in $A_8Tl_{11}X$ (A = K, Rb, Cs; X = Cl, Br). *Proceedings* **2018**, *2*, 1124. [CrossRef]
18. Gärtner, S.; Tiefenthaler, S.; Korber, N.; Stempfhuber, S.; Hischa, B. Structural Chemistry of Halide including Thallides $A_8Tl_{11}X_{1-n}$ (A = K, Rb, Cs; X = Cl, Br; n = 0.1–0.9). *Crystals* **2018**, *8*, 319. [CrossRef]
19. Falk, M.; El Addad, A.; Röhr, C. Crystal and electronic structure of alklai triele halogenides of the K8In11-type structure. In Proceedings of the 25th Annual Conference of the German Crystallographic Society, Karlsruhe, Germany, 27–30 March 2017; p. 112.
20. Häussermann, U.; Svensson, C.; Lidin, S. Tetrahedral stars as flexible basis clusters in sp-bonded intermetallic frameworks and the compound $BaLi_7Al_6$ with the $NaZn_{13}$ structure. *J. Am. Chem. Soc.* **1998**, *120*, 3867–3880. [CrossRef]
21. Dong, Z.C.; Corbett, J.D. $K_{18}Tl_{20}Au_3$-A Novel Derivative of K_8Tl_{11} with the Unprecedented Polyanion $Tl_9Au_2^{9-}$, the Parent Tl_{11}^{7-}, and an Isolated Au^- Ion. *Inorg. Chem.* **1995**, *34*, 5042–5048. [CrossRef]
22. Tillard-Charbonnel, M.; Chahine, A.; Belin, C.; Rousseau, R.; Canadell, E. Structure and chemical bonding in $K_{14}Cd_9Tl_{21}$, a compound containing both isolated Tl_{11}^{7-} clusters and $_\infty{}^2$ $[Cd_9Tl_{10}^{7-}]$ metallic layers. *Chem. Eur. J.* **1997**, *3*, 799–806. [CrossRef]
23. Cordier, G.; Müller, V. Preparation and crystal structure of $K_{49}Tl_{108}$. *Z. Naturforsch. B* **1993**, *48*, 1035–1040. [CrossRef]
24. Baden, W.; Schmidt, P.C.; Weiss, A. The Intermetallic System $LiCd_{1-x}Tl_x$. *Phys. State Sol. A* **1979**, *51*, 183–190. [CrossRef]
25. Tiefenthaler, S.M.; Schlosser, M.; Pielnhofer, F.; Shenderovich, I.G.; Pfitzner, A.; Gärtner, S. Investigations on Tetragonally Distorted Sodium Thallide NaTl-tI8. *Z. Anorg. Allg. Chem.* **2020**, *646*, 82–87. [CrossRef]

26. Tiefenthaler, S.; Korber, N.; Gärtner, S. Synthesis of the Tetragonal Phase of Zintl's NaTl and Its Structure Determination from Powder Diffraction Data. *Materials* **2019**, *12*, 1356. [CrossRef] [PubMed]
27. Evers, J.; Oehlinger, G. After more than 60 years, a new NaTl type Zintl phase: KTl at high pressure. *Inorg. Chem.* **2000**, *39*, 628–629. [CrossRef] [PubMed]
28. Evers, J. High Pressure Investigations of AIBIII Zintl Compounds (AI = Li to Cs; BIII = Al to Tl) up to 30 GPa. In *Zintl Phases-Principles and Recent Developments*, 1st ed.; Structure and Bonding; Fässler, T.F., Mingos, D.M.P., Eds.; Springer: Berlin/Heidelberg, Germany, 2011; Volume 139, pp. 57–96.
29. Cordier, G.; Müller, V.; Fröhlich, R. Crystal structure of potasium thallide (49/108), $K_{49}Tl_{108}$. *Z. Kristallogr.* **1993**, *203*, 148–149. [CrossRef]
30. Hackspill, L. Sur quelques properiétés des métaux alcalins. *Helv. Chim. Acta* **1928**, *11*, 1003–1026. [CrossRef]
31. Schneider, M.W.; Oppel, I.M.; Griffin, A.; Mastalerz, M. *CrysAlisPRO, 171.41.93a*; Oxford Diffraction/Agilent Technologies UK Ltd.: Yarnton, UK, 2020.
32. Dolomanov, O.V.; Bourhis, L.J.; Gildea, R.J.; Howard, J.A.K.; Puschmann, H. OLEX2: A complete structure solution, refinement and analysis program. *J. Appl. Cryst.* **2009**, *42*, 339–341. [CrossRef]
33. Sheldrick, G.M. Crystal structure refinement with SHELXL. *Acta Crystallogr. Sect. C-Struct. Chem.* **2015**, *71*, 3–8. [CrossRef]
34. Sheldrick, G.M. SHELXT-Integrated space-group and crystal-structure determination. *Acta Crystallogr. Sect. A* **2015**, *71*, 3–8. [CrossRef]
35. Brandenburg, K. *Diamond, 4.6.6*; Crystal Impact GbR: Bonn, Germany, 2021.
36. Toombs, A. *STOE WinXPOW, 3.4.6*; STOE & Cie GmbH: Darmstadt, Germany, 2016.